Positron scattering from Mg atoms

G.F. Gribakin and W.A. King

Abstract: Scattering of low-energy positrons from Mg atoms is considered using many-body theory methods. For the first time the contribution of the Ps-formation channel is taken into account in addition to the polarization potential of the atom. At low energies the virtual Ps formation creates a strong attraction in the positron–atom channel, which produces positron–atom bound states in the s and p waves (0.985 and 0.159 eV are the corresponding binding energies), and a low-lying d-wave resonance at 1 eV. At higher energies this contribution gives rise to an effective positron–atom repulsion. On the whole, the inclusion of the Ps-formation contribution drastically changes the behaviour of the phase shifts and the shape of the partial-wave cross sections below 20 eV. Total and inelastic positron–Mg cross sections have been calculated. It appears that the present theory can explain the very recent results of the first experiment on positron–Mg scattering.

Résumé : À l'aide de méthodes à N-corps, nous étudions la diffusion de positrons de basse énergie sur du Mg atomique. Pour la première fois il est tenu compte du canal de formation de positronium (Ps) en plus de celui de polarisation de l'atome cible. À basse énergie, la formation de Ps virtuel crée un fort champ attractif entre le positron et l'atome, donnant des état liés pour le système e^+–Mg dans les ondes s et p (à respectivement 0,985 et 0,159 eV) ainsi qu'une résonance dans l'onde d à 1.0 eV. À plus haute énergie, l'effet est répulsif. Globalement, l'inclusion de la formation de Ps affecte dramatiquement le calcul des déphasages et la forme des sections efficaces partielles sous 20 eV. Nous avons calculé les sections efficaces inélastique et totale de la réaction e^+ sur Mg. Notre théorie apparaît capable d'expliquer les résultats récents de la première expérience effectuée sur cette réaction.

[Traduit par la rédaction]

1. Introduction

The interaction of low-energy positrons with atoms has always been known to be a very interesting process to study. Although being different to electron scattering only in the sign of the projectile charge, positron scattering is physically richer. Namely, it has a specific rearrangement collision channel corresponding to the formation of positronium (Ps) that opens at energy $I + E_{1s}$ (I is the atomic ionization potential, and $E_{1s} = -6.8$ eV is the ground-state Ps energy). For many atoms, e.g., the alkalies, the ionization potential is smaller than 6.8 eV, which means that the Ps-formation channel is open at any positron energy, and hence can by no means be neglected. For atoms with $I > 6.8$ eV there is an energy range between 0 and $I + E_{1s}$ where the rearrangement channel is closed. However, the process of Ps formation still takes place virtually, and strongly influences the positron–atom interaction and the elastic scattering. It creates an additional attraction between the positron and the atom. Let us have a closer look at this interaction.

In the static approximation the charge distribution of a neutral atom produces a completely repulsive short-range potential for the positron. The polarization of the atom by the Coulomb field of the positron (dipole polarization dominates this effect at large positron–atom distances), gives rise to an attractive *polarization potential*. This potential has the asymptotic behaviour $-\alpha e^2/2r^4$ (α is the atomic dipole polarizability), and is quite similar to that acting between an atom and an electron, apart from the lack of exchange effects for positrons. However, the application of the same approximation, which accounts for the polarization of the target, to electron and positron scattering shows that in the positron case this approximation is clearly deficient (see, for example, ref. 1). There is another mechanism that contributes to the positron–atom interaction. It is virtual Ps formation. The use of many-body theory methods allows one to describe the projectile–atom interaction by means of a nonlocal energy-dependent correlation potential. This includes both the effects of polarization and Ps formation. In ref. 1 it is shown that the latter contributes about 30% and 20% of the total positron–atom correlation potential for H and He, respectively.

Drawing the comparison between electrons and positrons further we must say that until recently only electrons were thought to be able to form bound states with neutral atoms (negative ions). The polarization potential is known to play a very important role in this binding, and a proper account of electron correlations is crucial for obtaining correct electron affinities. Although positions are originally "handicapped" by the static atomic repulsion, they are favoured by the absence of the Pauli exclusion principle, and by the additional attraction due to virtual Ps formation. Therefore, it is not entirely unphysical, although quite surprising, that bound positron–atom states could exist [2]. Many-body theory calculations performed in that work showed that if an atom has a large dipole polarizability, the positron–atom polarization potential creates a low-lying virtual s level. This level is turned into a true bound state when the Ps-formation contribution is added to the correlation potential. For the four atoms considered (Mg, Zn, Cd, and Hg) the binding energies of 0.87, 0.23, 0.35, and 0.045 eV, respectively, were obtained. Despite the considerable effort towards proving or disproving

Invited paper/Article sollicité

Received August 21, 1995. Accepted February 20, 1996.

G.F. Gribakin[1] and W.A. King. School of Physics, University of New South Wales, Sydney 2052, Australia.

[1] **Phone:** +61 (2) 385 4605; **FAX:** +61 (2) 385 6060; **e-mail:** gribakin@newt.phys.unsw.edu.au

the existence of positron–atom bound states [3–6], Mg, Zn, Cd, and Hg have not been tried as candidates for binding. This is also true for many other atoms which, as estimates show [2], could have bound states with positrons.

Of course, due to the extreme importance of correlation effects the calculation of a bound positron–atom state is a difficult theoretical problem. Likewise, it is probably not easy to discover them experimentally (one suggestion would be to detect electromagnetic quanta with $\hbar\omega > E$ from the photo-attachment process in the positron–atom scattering at energy E). On the other hand, rather accurate measurements of low-energy positron scattering are feasible (see, for example, ref. 7). Such experiments could indirectly indicate the presence or absence of positron–atom bound states.

We would like to remind the reader that bound-state and scattering problems are in no way independent. For example, Levinson's theorem relates the value of the phase shift $\delta_l(k)$ at zero projectile moments k to the number n_l of bound states in a given partial wave for potential scattering ($\delta_l(0) = \pi n_l$, if $\delta_l(\infty) = 0$). Another example is the relation between the scattering length a ($\delta_0(k) = -ak$ for small k) and the position of a virtual or bound s level: if the scattering length is large compared to the size of the target, then for $a < 0$ a virtual level exists at $E = \hbar^2/2ma^2$, and for $a > 0$, there is a bound state at $E = -\hbar^2/2ma^2$.

Very recently a measurement of the total and Ps-formation cross section has been performed [8][2] for Mg at positron energies above 1 eV. The main purpose of the present work is to apply the same many-body theory approach used for the calculation of the positron–Mg bound state [2], to the scattering of positrons by Mg atoms. A comparison of the present results with the experimental scattering data would then be a test of the approach on the whole, and thus, may indirectly support the existence of positron–atom bound states.

The ionization potential of Mg ($I = 7.646$ eV) is rather small, and the Ps-formation threshold is just 0.8 eV from the atomic ground state. Firstly, this makes the effects of Ps formation of paramount importance. Secondly, above this energy the inelastic channel opens. For this reason we use in this work a slightly different numerical technique than in ref. 2, which enables us to calculate the correlation potential above the inelastic thresholds (both that of Ps formation and atomic excitations), where the correlation potential acquires an imaginary part. This technique also provides the real and imaginary parts of the phase shifts above the inelastic threshold, so that the elastic, inelastic, and total cross sections can be calculated for each of the positron's partial waves (s, p, d, f, and g).

2. Theoretical background

2.1. Basic equations

Within atomic many-body theory the problem of the interaction of a ground-state atom with a positron (or an electron) can be reduced to the single-particle Dyson equation (see, for example, ref. 9)

$$H_0\psi_E(\boldsymbol{r}) + \int \Sigma_E(\boldsymbol{r}, \boldsymbol{r}')\psi_E(\boldsymbol{r}')\,d\boldsymbol{r}' = E\psi_E(\boldsymbol{r}) \tag{1}$$

[2] W.E. Kauppila. Private communication.

where ψ_E is the quasi-particle wave function describing the motion of the extra particle of energy E, H_0 is the single-particle Hamiltonian (usually, the Hartree–Fock Hamiltonian of the atom), and Σ_E is a nonlocal energy-dependent potential, which describes the correlation interaction between the extra particle and the atom. It is equal to the self-energy operator of the single-particle Green's function, and contains all the necessary information about the many-body dynamics of the system. For small projectile energies $|E| \ll I$ the correlation potential has the well-known long-range asymptotic behaviour

$$\Sigma_E(\boldsymbol{r}, \boldsymbol{r}') \sim -\frac{\alpha e^2}{2r^4}\delta(\boldsymbol{r} - \boldsymbol{r}') \tag{2}$$

Solving (1) at $E > 0$ one can obtain the scattering phase shifts and calculate the cross sections. If (1) has a negative eigenvalue $E = \epsilon_0 < 0$, a positron–atom bound state (or a stable negative ion) exists.

It is convenient for numerical applications to solve the Dyson equation using a representation of eigenfunctions $\varphi_\epsilon(\boldsymbol{r})$ of the Hartree–Fock Hamiltonian H_0,

$$H_0\varphi_\epsilon(\boldsymbol{r}) = \epsilon\varphi_\epsilon(\boldsymbol{r}) \tag{3}$$

rather than in the coordinate representation (1). Due to the static repulsion produced by the atomic ground state, the spectrum of (3) is purely continuous for positrons. For atoms with closed shells H_0 is spherically symmetric, and without any additional approximations $\varphi_\epsilon(\boldsymbol{r})$ with definite orbital angular momentum l can be chosen. The latter is also true for $\psi_E(\boldsymbol{r})$, since the correlation interaction $\Sigma_E(\boldsymbol{r}, \boldsymbol{r}')$ with a spherically symmetric target does not violate the conservation of the projectile angular momentum. Equation (1) can be reformulated for bound-state problems as [10]

$$\epsilon C_\epsilon + \int \langle\epsilon|\Sigma_E|\epsilon'\rangle C_{\epsilon'}\,d\epsilon' = \epsilon_0 C_\epsilon, \qquad E = \epsilon_0 \tag{4}$$

where

$$C_\epsilon = \int \varphi^*_\epsilon(\boldsymbol{r})\psi_0(\boldsymbol{r})\,d\boldsymbol{r} \tag{5}$$

are the projections of the bound-state wave function $\psi_0(\boldsymbol{r})$, and $\langle\epsilon|\Sigma_E|\epsilon'\rangle$ is the matrix element of the correlation potential in a given partial wave:

$$\langle\epsilon|\Sigma_E|\epsilon'\rangle = \int \varphi^*_\epsilon(\boldsymbol{r})\Sigma_E(\boldsymbol{r}, \boldsymbol{r}')\varphi_{\epsilon'}(\boldsymbol{r}')\,d\boldsymbol{r}\,d\boldsymbol{r}' \tag{6}$$

We should mention that due to the energy dependence of Σ_E (4) must be solved by iterations, i.e., using the negative eigenvalue ϵ_0 as the energy to calculate Σ_E at, and repeating this procedure until $\epsilon_0 = E$ is achieved.

The self-energy matrix $\langle\epsilon|\Sigma_E|\epsilon'\rangle$ can also be used to calculate the phase shifts directly. This requires the following matrix equation [11] to be solved:

$$\langle\epsilon|\tilde{\Sigma}_E|\epsilon'\rangle = \langle\epsilon|\Sigma_E|\epsilon'\rangle + \int \frac{\langle\epsilon|\tilde{\Sigma}_E|\epsilon''\rangle\langle\epsilon''|\Sigma_E|\epsilon'\rangle}{E - \epsilon''}\,d\epsilon'' \tag{7}$$

The phase shift is then obtained as

Fig. 1. The main contribution to the positron–atom polarization potential $\langle\epsilon'|\Sigma_E^{\rm pol}|\epsilon\rangle$. The thick lines describe positron states, the thin lines are electron and hole states, and the double line corresponds to the electron state ν_2 calculated in the field of the hole n.

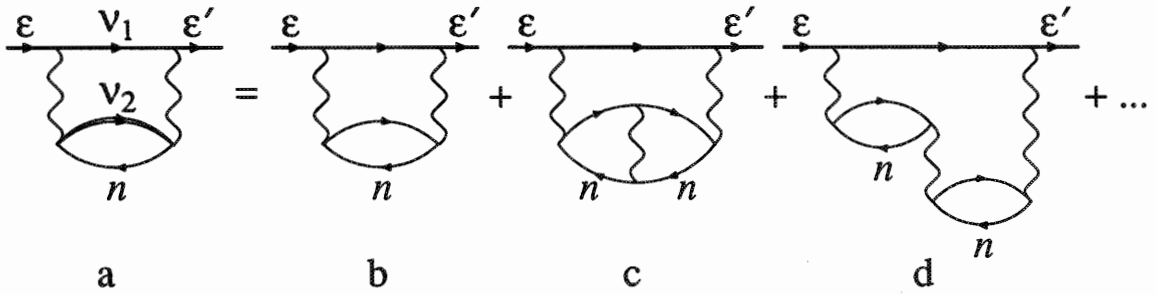

$$\delta_l(k) = \delta_l^{\rm HF}(k) + \Delta\delta_l(k) \tag{8}$$

$$\Delta\delta_l(k) = \tan^{-1}[-\pi\langle\epsilon|\tilde{\Sigma}_\epsilon|\epsilon\rangle] \tag{9}$$

where $\delta_l^{\rm HF}(k)$ is the Hartree–Fock phases shift, $\Delta\delta_l(k)$ is the additional phase shift due to the correlation potential, and $\epsilon = k^2/2$ is the projectile energy (atomic units are used throughout). If the correlation potential $\Sigma_E(\boldsymbol{r}, \boldsymbol{r}')$ is not strong, the additional phase shift is small and can be found by perturbations as $\Delta\delta_l(k) \simeq -\pi\langle\epsilon|\Sigma_\epsilon|\epsilon\rangle$ (in this case $\tilde{\Sigma}_E \simeq \Sigma_E$, which corresponds to the distorted-wave Born approximation applied to $\Sigma_E(\boldsymbol{r}, \boldsymbol{r}')$, when the second term on the right-hand side of (7) can be neglected). It becomes especially transparent in this limit that if the diagonal matrix element of the correlation potential is negative, the correlation potential increases the phase shift, which means effective attraction, and if $\langle\epsilon|\Sigma_\epsilon|\epsilon\rangle > 0$, the correlation potential is effectively repulsive.

When the energy E is greater than the lowest of the inelastic thresholds (either the Ps-formation threshold $I - 6.8$ eV, or the atomic excitation threshold), the correlation potential Σ_E acquires an imaginary part, and the phase shifts obtained from (7)–(9) become complex: $\delta_l = \delta_l' + i\delta_l''$ ($\delta_l'' > 0$, as follows from the unitarity condition). The elastic, inelastic, and total scattering cross sections are obtained by summing over the partial waves:

$$\sigma_{\rm el} = \frac{4\pi}{k^2}\sum_{l=0}^{\infty}(2l+1)\,{\rm e}^{-2\delta_l''}\,(\sin^2\delta_l' + \sinh^2\delta_l'') \tag{10}$$

$$\sigma_{\rm in} = \frac{\pi}{k^2}\sum_{l=0}^{\infty}(2l+1)(1-{\rm e}^{-4\delta_l''}) \tag{11}$$

$$\sigma_{\rm tot} = \sigma_{\rm el} + \sigma_{\rm in} = \frac{2\pi}{k^2}\sum_{l=0}^{\infty}(2l+1)(1-{\rm e}^{-2\delta_l''}\cos 2\delta_l') \tag{12}$$

If the Ps-formation threshold is lower than the atomic excitation threshold (for Mg they are 0.843 and 4.35 eV, respectively), the inelastic cross section for positron energies between the thresholds (in the Ore gap) is equal to the Ps-formation cross section. At higher energies the present formalism cannot distinguish between different inelastic channels, and $\sigma_{\rm in}$ is the reaction cross section.

Provided the correlation potential is known exactly, the approach outlined above is exact. Atomic properties that can be calculated include the binding energies, positions of atomic thresholds, cross sections, etc. Thus, all the complexity of the many-body dynamics of the system is incorporated in Σ_E. However, in practice one has to use some approximations to calculate the correlation interaction. We address this question in the next section.

2.2. Correlation potential

Obviously, the most important point in applying many-body theory is the calculation of $\langle\epsilon'|\Sigma_E|\epsilon\rangle$. Theoretically, the self-energy can be presented as an infinite perturbation theory series in powers of the residual electron–electron and positron–electron Coulomb interaction. The easiest way of describing the items of this series is by using many-body theory diagrams (see, for example, refs. 9 or 12, for atomic applications).

Numerous calculations show (see, e.g., an early work by Kelly [13], or a recent paper [14] and references therein) that even the lowest order terms of the series (second-order diagrams) give a reasonable approximation for the correlation potential Σ_E, at least in the electron–atom case (Fig. 1*b* is the only second-order diagram for positron–atom interaction). This approximation yields the correct asymptotic behaviour (2), although α is different from the true atomic polarizability. A much more accurate approximation for Σ_E is achieved by summing certain subseries of higher order diagrams [12, 15, 16]. These diagrams are still of second order with respect to the projectile–target interaction; however, they include a large amount of electron correlations inside the target (Figs. 1*c*, 1*d*, and Fig. 2).

For example, the sum of the diagrams in the right-hand side of the diagrammatic equation (Fig. 1) can be included within the second-order diagram Fig. 1*a* by calculating the wave function of the excited electron ν_2 in the field of the hole in the orbital n coupled into a certain total angular momentum L [12]. In this case L is equal to the angular momentum transferred through the Coulomb interaction. Analytically, the contribution of this diagram to $\langle\epsilon'|\Sigma_E|\epsilon\rangle$ is given by

$$\langle\epsilon'|\Sigma_E^{\rm a}|\epsilon\rangle = \sum_{n\nu_1\nu_2}\frac{\langle\epsilon' n|V|\nu_2\nu_1\rangle\langle\nu_1\nu_2|V|n\epsilon\rangle}{E - \epsilon_{\nu_1} - \epsilon_{\nu_2} + \epsilon_n + i\delta} \tag{13}$$

Fig. 2. Third-order corrections to the positron–atom polarization potential.

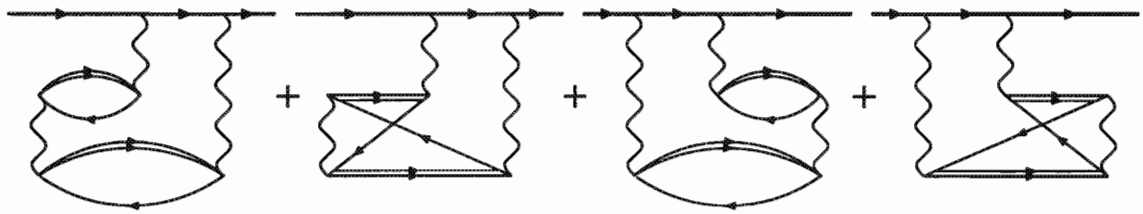

Fig. 3. The diagrams contributing to the Ps-formation potential $\langle\epsilon'|\Sigma_E^{\rm Ps}|\epsilon\rangle$. The shaded rectangle on the right-hand side of the diagrammatic equation describes the propagation of the correlated electron–positron pair.

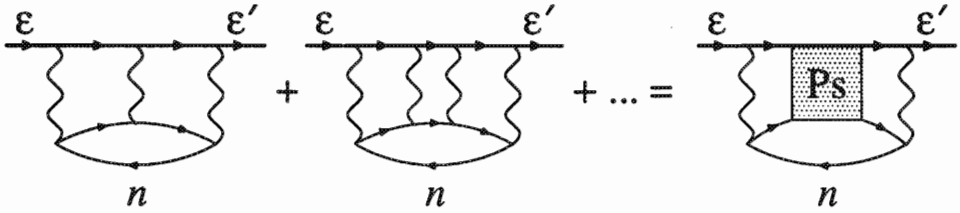

where V is the Coulomb interaction, the summation is carried over the intermediate positron, excited electron, and hole states, ν_1, ν_2, and n, respectively, and $i\delta$ in the denominator defines the integration path when the integral has a pole (this pole emerges in (13), if the projectile energy E is above the first excitation threshold of the target).

There are other important higher order diagrams (Fig. 2) that can be taken into account either approximately [16], as factors to multiply (13), or exactly [15], by using the Feynman diagram technique to calculate the renormalized polarization operator. On the whole, this approach provides accurate results for electron–atom scattering [11, 12, 14], negative-ion bound states [10, 14], and atomic energy levels [15]. For example, the calculated energy of the low-lying p-wave resonance in electron scattering from Mg[3]: 0.16 eV, is in good agreement with experimental values: 0.15 eV [17], and 0.16 ± 0.03 eV [18].

When applied to positron–atom scattering, the approximation described above for Σ_E (we will call it the *polarization potential* $\Sigma_E^{\rm pol}$, since it essentially accounts for the interaction due to the polarization of the target by the projectile) proved to be insufficient [19]. There it was shown that the possibility of Ps formation influences the positron–atom interaction even if the positron energy is below the Ps-formation threshold (virtual Ps formation). From the diagrammatic point of view this means that there is a certain sequence of diagrams (Fig. 3) that gives a sizeable contribution to Σ_E in the positron–atom case [1, 19]. Indeed, it is easy to verify that all diagrams on the left-hand side of the diagrammatic equation (Fig. 3) have the same sign, whereas in the electron–atom case this series is sign-alternating and apparently gives a small total. We call this contribution the *Ps-formation potential*, $\Sigma_E^{\rm Ps}$. The total positron–atom correlation potential is then calculated as the sum

$$\Sigma_E = \Sigma_E^{\rm pol} + \Sigma_E^{\rm Ps} \tag{14}$$

In ref. 1 we suggested an approximate way to calculate $\Sigma_E^{\rm Ps}$:

$$\langle\epsilon'|\Sigma_E^{\rm Ps}|\epsilon\rangle = \sum_n \int \frac{\langle\epsilon' n|V|\tilde{\Psi}_{1s,K}\rangle\langle\tilde{\Psi}_{1s,K}|V|n\epsilon\rangle}{E+\epsilon_n-\left(E_{1s}+\frac{K^2}{2M}\right)+i\delta}\,\frac{{\rm d}^3K}{(2\pi)^3} \tag{15}$$

where $V = -1/|\boldsymbol{r}-\boldsymbol{r}_1|$ is the electron–positron Coulomb interaction, $\Psi_{1s,K} = \varphi_{1s}(\boldsymbol{r}-\boldsymbol{r}_1)\,{\rm e}^{i\boldsymbol{K}\cdot\boldsymbol{R}}$ is the wave function of the Ps atom in the ground state, moving with momentum $\boldsymbol{K}$, $E_{1s}+K^2/2M$ is the energy of this state, M is the mass of the Ps atom, n is the hole state, and ϵ_n is its energy in the Hartree–Fock approximation. The tilde above $\Psi_{1s,K}$ indicates that this wave function is orthogonal to the single-electron states of the atomic ground state:

$$|\tilde{\Psi}_{1s,K}\rangle = (1-\Sigma_n|n\rangle\langle n|)|\Psi_{1s,K}\rangle$$

This is necessary since the shaded block in the right-hand side of the diagrammatic equation in Fig. 3 is constructed from the excited electron states. This shaded block describes the propagation of the correlated electron–positron pair (Ps). Obviously, approximation (15) neglects (virtual) Ps formation into excited states. Simple physical arguments and comparison with other numerical calculations show that this approximation can be justified for small- and medium-radius targets [1]. In accordance with that reasoning, the close-coupling calculations of Hewitt et al. [20] show a progressive increase of the excited Ps formation in the alkali atoms, Li, Na, and K, with the increase of atomic radius. Furthermore, since the radius of Mg is smaller than that of Li, the excited Ps formation should be of less importance.

By examining (15) one can get a clear insight into the role of Ps formation in positron–atom scattering. The matrix element $\langle\tilde{\Psi}_{1s,K}|V|n\epsilon\rangle$ is the lowest order amplitude of the formation of Ps($1s$) by a positron of energy ϵ and an electron from the atomic orbital n. Since low-energy positrons

[3] A.A. Gribakina and G.F. Gribakin. Unpublished.

do not penetrate far into the atom, this amplitude is maximal if n is the valence orbital. The outer valence orbital also gives the smallest energy difference $E_{1s} - \epsilon_n \simeq I - 6.8$ eV in the denominator (the binding energy of the outer electron $|\epsilon_n|$ is the Hartree–Fock value of the ionization potential). Thus, the sum over n is dominated by the valence orbital. It is evident that for $E < -\epsilon_n + E_{1s} \simeq I - 6.8$ eV the diagonal matrix element $\langle\epsilon|\Sigma_E^{\rm Ps}|\epsilon\rangle$ is negative. This means that the Ps-formation contribution in (14) corresponds to additional attraction. For $E > I - 6.8$ eV the integral over K in (15) has a pole, and the integrand is positive for small K, and negative for large K. In this case the Ps-formation contribution to Σ_E may become positive, thus acting as repulsion in the positron–atom channel. This situation is probably realized in positron collisions with alkali atoms ($I < 6.8$ eV). Indeed, the close-coupling calculation of Hewitt et al. [20] shows that the coupling to the Ps-formation channels reduces the $ns \rightarrow np$ excitation cross sections for Li, Na, and K by almost 50% at their maxima, suppresses the elastic cross section for K below 7 eV, and even reduces the total scattering cross section for K. These effects are also emphasized by comparison with experimental results [21]. It is worth noting that the presence of the pole in the integration over K in (15) gives rise to the imaginary part:

$$\mathrm{Im}\,\langle\epsilon|\Sigma_E^{\rm Ps}|\epsilon\rangle \propto |\langle\tilde{\Psi}_{1s,K}|V|n\epsilon\rangle|^2$$

If Σ_E is taken into account to first order (distorted wave Born approximation), this imaginary part is proportional to the Ps-formation cross section (the optical theorem).

Using (14) together with approximation (15) we calculated positron scattering from H and He [1], and obtained good agreement with the precise phase shifts from variational calculations for H, and with experimental data for He. It was also shown that the inclusion of $\Sigma_E^{\rm Ps}$ radically improves the agreement with experimental data for positron–noble-gas-atom scattering and annihilation.[4]

The calculations of low-energy positron scattering from Ne, Ar, Kr, and Xe[4] produced the scattering lengths of −0.43, −3.9, −9.1, and ~ -100 au, respectively. This indicates that for Ar, Kr, and Xe the positron–atom correlation potential creates virtual s levels at 1, 0.16, and 0.001 eV. Thus, it looked quite natural that when we considered the interaction of positrons with some other atoms that had larger dipole polarizabilities and smaller ionization potentials (Mg, Zn, Cd, and Hg), s-wave bound states were obtained [2]. In all cases the atomic ionization potentials are greater than 6.8 eV, and the attractive contribution of $\Sigma_E^{\rm Ps}$ to the correlation potential is very large.

3. Numerical calculations and results

The numerical calculations were performed using original codes and those based on ref. 22 in the following way.

- Calculation of the Mg ground state in the Hartree–Fock approximation.
- Calculation of the sets of positron states ϵ (l = 0–4) and v_1 (l = 0–5) in the static field of the ground-state atom, and excited electron states v_2 (l = 0, 1, 2) in the HF potential of Mg^+ $3s$ (only excitations from the valence $3s$ subshell of Mg have been taken into account).
- Calculation of the Coulomb matrix elements $\langle \mathrm{v}_1\mathrm{v}_2|V|n\epsilon\rangle$ and $\langle\tilde{\Psi}_{1s,K}|V|n\epsilon\rangle$.
- The self-energy matrix $\langle\epsilon|\Sigma_E|\epsilon'\rangle$, calculated by summation over the intermediate states at different E ((13)–(15)) is used to solve the bound-state problem (4), and to calculate the phase shifts from (7)–(9).
- Using the phase shifts the cross sections are obtained from (10)–(12).

We should note that to calculate $\Sigma_E^{\rm pol}$ from (13) and to solve (4) and (7) the positron and electron continuous spectra were discretized, and all integrations over the continua were replaced by summation over sets of states equidistant in momentum k. The following grids were used to ensure smooth variation of the integrands and convergence of sums. Positron states ϵ: $\Delta k = 0.03$, 59 points; v_1: 25 points with $\Delta k = 0.02$ or 0.03, spanning small-energy region, and 25 states with $\Delta k = 0.1$ at higher energies. Electron excited states v_2: four discrete nl excitations, and 25 continuous spectrum states with $\Delta k = 0.1$.

If approximation (13) is used for $\Sigma_E^{\rm pol}$, the asymptotic behaviour (2) corresponds to the Hartree–Fock dipole polarizability of the atom. For Mg the latter is $\alpha_{\rm HF} \simeq 100$ au^2, which considerably overestimates the accepted polarizability of Mg, $\alpha = 72$ au [23]. The accuracy of the polarization potential (13) can be improved by including the third-order diagrams (Fig. 2), thus taking double-electron excitations into account. The latter are especially important for the dipole excitations of the atom, which give a dominant contribution to $\Sigma_E^{\rm pol}$ (see Table 1). In this work we included the diagrams in Fig. 2 into $\Sigma_E^{\rm pol}$ by multiplying the dipole contribution in (13) by the factor

$$1 - \frac{1}{3}\,\frac{\langle 3s3p||V||3s3p\rangle}{\epsilon_{3p} - \epsilon_{3s}} \simeq 0.823 \qquad (16)$$

where $\langle 3s3p||V||3s3p\rangle$ is the reduced dipole Coulomb matrix element of the $3s^2 \rightarrow 3p^2$ excitation. This approximation for the third-order diagrams is in fact quite accurate because the $3s \rightarrow 3p$ dipole excitation gives about 90% of the dipole polarizability of Mg. The corrected polarizability $\alpha \simeq 82$ au is close to the value 81.16 au obtained in the polarized orbital approximation [24].[5]

The calculation of $\langle\tilde{\Psi}_{1s,K}|V|n\epsilon\rangle$ and $\langle\epsilon|\Sigma_E^{\rm Ps}|\epsilon'\rangle$ from (15) was done by expanding the Ps wave function $\Psi_{1s,K}$ in terms of spherical harmonics with respect to the nucleus. Angular momenta $l \leq 7$ were included. Integration over the angular variables was performed analytically, and that over radii and K, numerically, the continuous spectrum of K represented by 63 points with $\Delta K = 0.05$. We used the experimental energy $\epsilon_{3s} = -I$ in (15) to describe the position of the Ps-formation threshold correctly. This is essential for the calculation of $\langle\epsilon|\Sigma_E^{\rm Ps}|\epsilon'\rangle$ in Mg since the difference $\epsilon_{3s} - E_{1s} = -0.843$ eV is the denominator in quite small.

[4] V.A. Dzuba, V.V. Flambaum, G.F. Gribakin, and W.A. King. Manuscript in preparation.

[5] This approximation is equivalent to the RPA description of the excited atom, which corresponds to the summation of diagrams with electron–hole interactions (Figs 1*c*, 1*d*, and Fig. 2, etc.).

Table 1. Contributions of various diagrams to the self-energy matrix.

		$\langle\epsilon\|\Sigma_\epsilon^{pol}\|\epsilon\rangle$						$\langle\epsilon\|\Sigma_\epsilon^{Ps}\|\epsilon\rangle$	
		Monopole		Dipole		Quadrupole			
l	k^a	Re	Im	Re	Im	Re	Im	Re	Im
0	0.2	−0.0061	0.0000	−0.2095	0.0000	−0.0336	0.0000	−1.2628	0.0000
0	0.8	−0.0335	−0.0198	−0.1795	−0.0185	−0.0293	−0.0005	−0.0028	−0.0439
1	0.2	−0.0008	0.0000	−0.0928	0.0000	−0.0114	0.0000	−0.2322	0.0000
1	0.8	−0.0201	−0.0099	−0.1688	−0.0717	−0.0352	−0.0014	0.2368	−0.0691
2	0.2	-3×10^{-5}	0.0000	−0.0272	0.0000	−0.0019	0.0000	−0.0153	0.0000
2	0.8	−0.0070	−0.0027	−0.1290	−0.0836	−0.0363	−0.0098	0.2072	−0.1601
3	0.2	-5×10^{-7}	0.0000	−0.0098	0.0000	−0.0003	0.0000	−0.0007	0.0000
3	0.8	−0.0020	−0.0005	−0.0956	−0.0593	−0.0225	−0.0094	0.1067	−0.1261
4	0.2	Not calc.	Not calc.	−0.0045	0.0000	Not calc.	Not calc.	-3×10^{-5}	0.0000
4	0.8	Not calc.	Not calc.	−0.0678	−0.0300	Not calc.	Not calc.	0.0417	−0.0661

[a]The values of the positron momentum $k = 0.2$, 0.8 correspond to the positron energies of 0.544 and 8.708 eV, respectively.

The results of our calculations are presented in Figs. 4–6 and Tables 1 and 2. To get a better understanding of the role of correlation effects, and to appreciate the effect of Ps formation on positron–Mg scattering, we take into account the polarization potential alone first, and then add the Ps-formation potential.

Table 1 allows one to compare the contributions of different atomic excitations to the polarization potential for different projectile orbital momental l. The two values of the positron momenta are chosen so that for the first one ($k = 0.2$) elastic scattering is the only open channel ($\mathrm{Im}\Sigma_E = 0$), whereas the second value ($k = 0.8$) lies above both the Ps-formation and the atomic excitation and (or) ionization thresholds ($\mathrm{Im}\Sigma_E^{Ps}$, $\mathrm{Im}\Sigma_E^{pol} \neq 0$). It is clear that the dipole atomic excitations dominate in Σ_E^{pol}. For example, they give 84% of Σ_E^{pol} for $l = 0$, $k = 0.2$, while the monopole and quadrupole excitations account for about 2 and 14% of the polarization potential. We estimate that the neglect of higher angular momentum excitations of the atom corresponds to a few per cent accuracy of Σ_E^{pol}. In higher positron partial waves the dominance of the dipole contribution in Σ_E^{pol} becomes even more prominent at small energies. It is well known that the presence of the long-range $-\alpha/2r^4$ potential changes the low-energy expansion of the scattering phase shifts [25]:

$$\delta_0(k) = -ak - \frac{\pi\alpha k^2}{3} \tag{17}$$

$$\delta_l(k) = \frac{\pi\alpha k^2}{(2l-1)(2l+1)(2l+3)}, \qquad l \geq 1 \tag{18}$$

The anomalous quadratic term can be obtained in the Born approximation. Therefore, the polarization potential matrix element has the low-energy behaviour: $\langle\epsilon|\Sigma_\epsilon^{pol}|\epsilon\rangle \sim -\alpha k^2/[(2l-1)(2l+1)(2l+3)]$, $l \geq 1$. The range of validity of (18) increases with l, e.g., for the f-wave phase shift produced by Σ_E^{pol} (18) holds up to $k \sim 0.6$ with $\alpha \simeq 80$ (see Fig. 4). Thus, we can check the accuracy of the numerically calculated polarization potential in the asymptotic region without actually probing the behaviour of the nonlocal radial potential (2).

Above the first atomic excitation threshold ($k > 0.55$) an imaginary part emerges in Σ_E^{pol}. On the whole, it is also dominated by the dipole excitations. On the other hand, the relative importance of the quadrupole contribution in Σ_E^{pol} increases at larger energies, which is more noticeable for higher positron angular momenta.

The momentum dependence of the phase shifts obtained from Σ_E^{pol} (Fig. 4, open symbols) shows that the positron–Mg polarization potential alone is quite strong, since the phase shifts are very different from those produced by the static atomic potential. Gradually, as the energy increases, they tend to follow the static phase shifts, although even at the rightmost boundary ($E = 39$ eV) the effect of the polarization potential on the phase shifts is quite prominent.

The s phase shift varies very rapidly near the origin, and this does not allow a precise determination of the scattering length. Its estimated value $a \sim -60$ (the same scattering length was obtained for Σ_E^{pol} in ref. 2) corresponds to a virtual level at 4 meV. Just as in our previous calculation the polarization potential is not strong enough to form a bound positron–atom state. This is in disagreement with the results of Szmytkowsky [26] who obtained positron–Mg binding of 0.02 eV by calculating the positron–atom potential using the polarized orbital approximation. The polarized-orbital potential can be obtained from our Σ_E^{pol}, if the adiabatic approximation for the projectile is used. The latter essentially corresponds to the neglect of E and ϵ_{v_1} in the denominator of (13) and analogous approximations in the diagrams of Fig. 2. This approximation makes the polarization potential local and energy-independent, and clearly overestimates Σ_E^{pol} at small E, since the absolute values of the energy denomi-

Fig. 4. The positron–Mg s, p, d, and f scattering phase shifts. Open symbols, only the polarization potential taken into account: $\Sigma_E = \Sigma_E^{\rm pol}$ (inelastic threshold at $k = 0.55$). Solid symbols, with the Ps-formation contribution added to the correlation potential: $\Sigma_E = \Sigma_E^{\rm pol} + \Sigma_E^{\rm Ps}$ (inelastic threshold at $k = 0.25$). Squares, Re δ_l; triangles, Im δ_l; and broken-line curve, Hartree–Fock phase shifts.

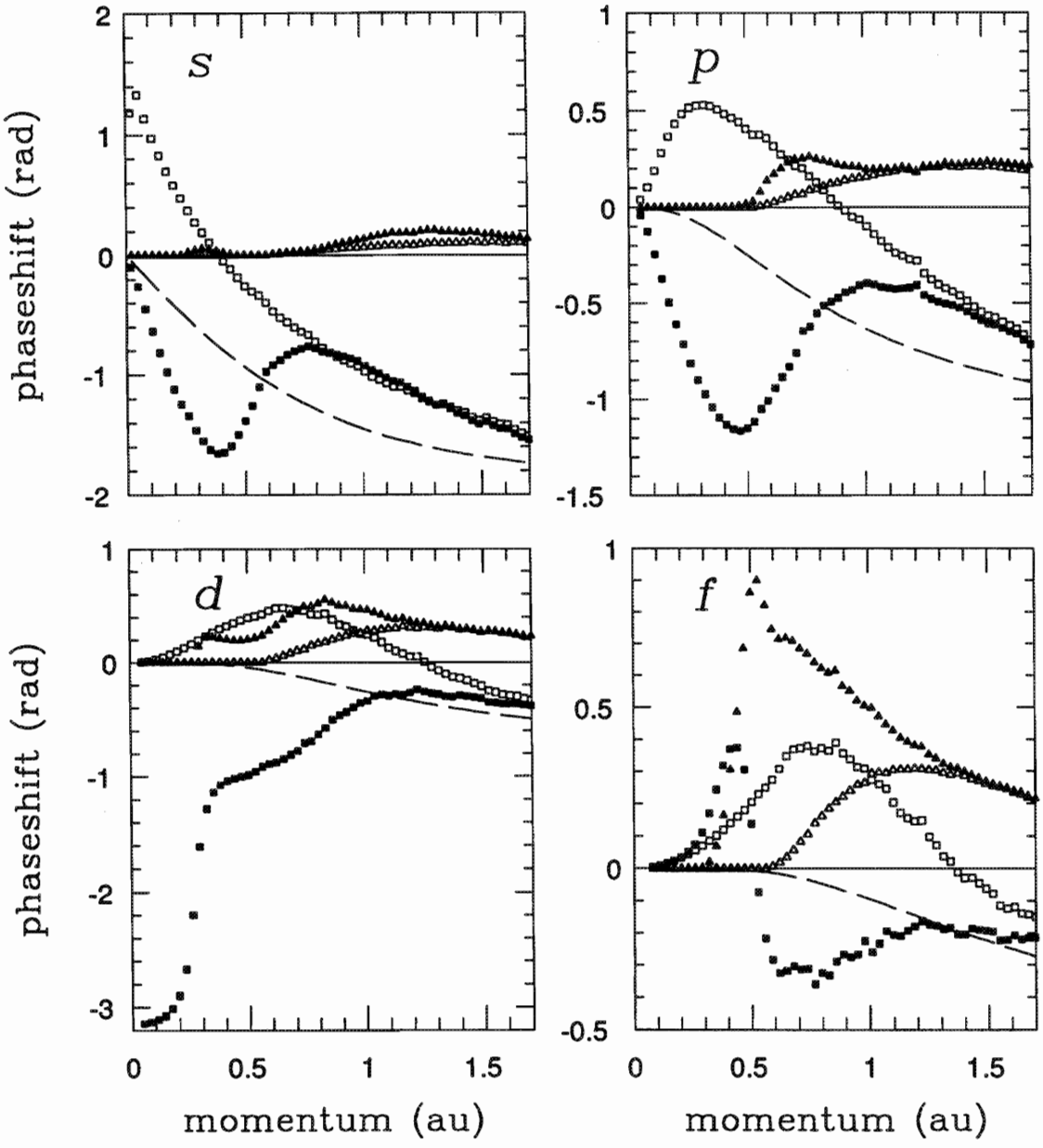

nators are underestimated by the neglect of the intermediate positron energies (for example, ϵ_{ν_1} in (13)).

Above $k = 0.55$ the phase shifts acquire quite a substantial imaginary part: Im $\Delta\delta_l \sim$ Re $\Delta\delta_l$ at $k \sim 1$, which means large atomic excitation and (or) ionization probabilities (Fig. 4, open triangles). These processes produce a clear onset in the total scattering cross section (Fig. 6*a*). Otherwise, the cross section is monotonically decreasing, in qualitative agreement with the polarized-orbital calculation [26]. One can see from Fig. 6*a* that five partial waves (l = 0–4) are by no means enough to get convergence of the cross section at $k \gtrsim 1$. However, the addition of the higher partial waves would not change the overall shape of the cross section. Instead, it will smoothly lift the high-energy tail of $\sigma_{\rm tot}$ above the one shown in Fig. 6*a*.

The addition of the Ps-formation potential $\Sigma_E^{\rm Ps}$ produces drastic changes in the whole picture of positron–Mg scattering. These changes are caused by the large magnitude of $\Sigma_E^{\rm Ps}$ (see Table 1). Apparently, for small positron energies the additional attraction due to $\Sigma_E^{\rm Ps}$ is comparable in magnitude with $\Sigma_E^{\rm pol}$. The strength of the nonlocal potential Σ_E can be better characterized by the quantity $-{\rm Tr}(G\Sigma)$, which enters the necessary condition for a nonlocal potential to create a bound state [14]:

Fig. 5. The wave functions of the bound positron–Mg states. Continuous line, s state ($\epsilon_0 = -0.985$ eV); broken line, p state ($\epsilon_0 = -0.159$ eV).

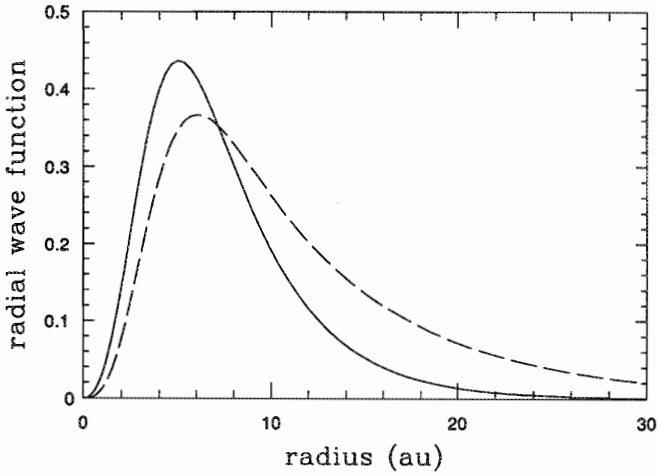

$$-\mathrm{Tr}(G\Sigma) \equiv -\int \frac{\langle\epsilon|\Sigma_{E=0}|\epsilon\rangle}{\epsilon}\,\mathrm{d}\epsilon > 1 \qquad (19)$$

where $G = (E - H_0)^{-1}$ is the Green function of the projectile in the static field of the target, and both G and Σ in (19) are taken at zero energy. The polarization and Ps formation contribute additively to Σ_E and to the left-hand side of criterion (19). For the s wave these contributions are 1.16 and 3.02, respectively. These values reveal several things. First, Σ_E^{pol} alone satisfies (19). However, this is only a necessary condition, and we know that there is no binding in Σ_E^{pol}, yet this contribution produces an "almost bound" state: a low-lying virtual level. Second, the strength of Σ_E^{Ps} at $E = 0$ for the s wave is even greater than that of Σ_E^{pol}. Third, the large total value $-\mathrm{Tr}(G\Sigma) = 4.18$ makes the existence of the s bound state almost certain. Indeed, (4) solved with Σ_E from (14) yields $\epsilon_0 = -0.985$ eV. The corresponding positron wave function is shown in Fig. 5. The above value of ϵ_0 is rather close to the one we obtained earlier [2]: $\epsilon_0 = -0.87$ eV. This difference is mainly due to the different methods of calculating Σ_E^{pol}.

When applied to the p-wave correlation potential, the values of $-\mathrm{Tr}(G\Sigma) = 0.54$ and 1.02 for Σ_E^{pol} and Σ_E^{Ps} are obtained, respectively. Hence, there is certainly no p binding if only the polarization potential is included. For the total correlation potential ($-\mathrm{Tr}(G\Sigma) = 1.56$) (4) yields a negative value $\epsilon_0 = -0.159$ eV (see the positron radial wave function in Fig. 5). The p binding energy was not calculated in ref. 2, although it has been checked, the approximation used there also produces p binding. Of course, the smaller magnitude of the p binding energy makes our prediction less reliable.

The phase shifts produced by the total correlation potential $\Sigma_E^{\mathrm{pol}} + \Sigma_E^{\mathrm{Ps}}$ are shown in Fig. 4 by solid symbols. Despite a considerable difference between the s, p, d, and f phase shifts, they all have a common feature: as the positron momentum increases above some value ($k \sim 1$) the phase shifts produced by the total correlation potential become close to those given by the polarization potential alone. Note that this is true for both the real and the imaginary parts of $\delta_l(k)$. This means that at larger energies the Ps-formation potential becomes small in comparison with the polarization potential (the larger the orbital angular momentum, the larger is the k value where this happens). In fact, we used this property when plotting the phase shifts to overcome the usual mod π ambiguity. Examining the deviation of Re $\delta_l(k)$ produced by $\Sigma_E^{\mathrm{pol}} + \Sigma_E^{\mathrm{Ps}}$ from that due to Σ_E^{pol} towards smaller values of k, one can see that in that energy range Σ_E^{Ps} acts as a repulsion, since its inclusion into the correlation potential brings the real parts of the phase shifts closer to the HF values.

At even smaller energies ($k < 0.5$) the behaviour of the s and p phase shifts, the d phase shift, and the f phase shift are very different. This difference reflects the diversity of physical effects produced by the now strong *attractive* Ps-formation potential (it is easy to check that below the Ps-formation threshold, at $k < 0.25$, the diagonal matrix element of Σ_E^{Ps} from (15) is strictly negative, which means attraction). The way the s- and p-wave phase shifts approach zero reflects the existence of bound states. Thus, the positive scattering length of $a \approx 4.2$ gives the following estimate of the s binding energy: $|\epsilon_0| \approx \hbar^2/2ma^2 \approx 0.8$ eV, which is close to that obtained from (4) ($|\epsilon_0| = 0.985$ eV). The positron–atom attraction in the d wave is not strong enough to form a bound state. However, it produces a resonance at $k \approx 0.27$, where the phase shift passes through $-\pi/2$. For higher partial waves (f, g) the effect of the Ps-formation potential on the real part of the phase shift is probably not as dramatic as for $l = 0$, 1, and 2. On the other hand, Σ_E^{Ps} produces very large imaginary phase shifts. Thus, its maximal value for the f wave is $\mathrm{Im}\delta_3 = 0.9$ at $k = 0.53$, and for the g wave, $\mathrm{Im}\delta_4 = 0.35$ at $k = 0.9$.

We would like to mention that the observed behaviour of the s, p, and d phase shift clearly contradicts Levinson's theorem. If the theorem had been fulfilled, the s and p phase shifts would have reached π values, and the d phase shift would have gone to zero at $k = 0$. This violation should not be considered as a worry, since the theorem itself has been proven for potential scattering by an energy-independent potential. Nevertheless, in the electron–atom problems where negative-ion bound states are present, Levinson's theorem always seemed to be fulfilled [10, 16], probably because the energy dependence of Σ_E^{pol} is much weaker than that of Σ_E^{Ps}. Apart from the very strong energy dependence of Σ_E^{Ps}, which is attractive at small energies and repulsive at higher energy, the existence of the Ps bound state itself is an additional complication of the standard conditions for Levinson's theorem.

Another effect due to the Ps-formation channel is related to the behaviour of the phase shifts in the vicinity of the atomic excitation threshold ($k = 0.55$). It appears that for the s and p waves the increase of $\mathrm{Im}\delta_l$ corresponding to the atomic excitation processes becomes somewhat greater when the Ps-formation potential is included. In the d wave, the corresponding onset has about the same magnitude as that obtained from Σ_E^{pol}, whereas for the f (and g) wave the behaviour of $\mathrm{Im}\delta_l$ above $k = 0.55$ hardly reveals any channel-opening effects at all. The latter means that the inclusion of the Ps-formation channel in the calculation suppresses the atomic excitation cross section near the threshold. Accordingly, there is no visible feature in the total cross section

Fig. 6. The positron–Mg total scattering cross sections: (*a*) when only the polarization potential is taken into account; (*b*) when the Ps-formation contribution is added. The partial cross sections: *s*, thin continuous line; *p*, broken line; *d*, dot–dash curve; *f*, long dash – short dash; and *g*, dotted-line curve. The thick continuous line is the total cross section.

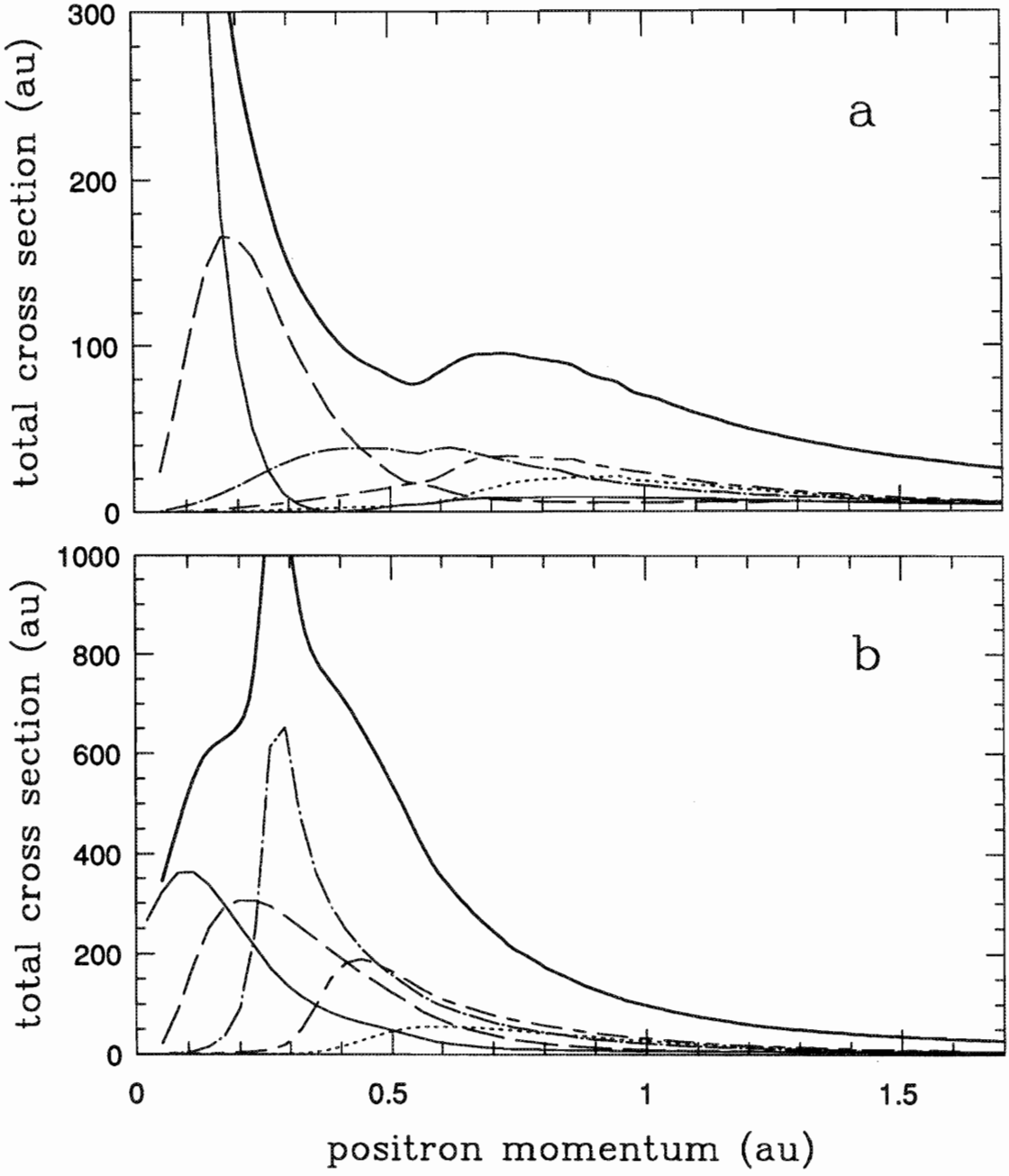

at $k = 0.55$ when the Ps formation is taken into account (Fig. 6*b*), contrary to the results from bare $\Sigma_E^{\rm pol}$ (Fig. 6*s*). A suppression of atomic excitation due to Ps channels was observed for $ns \rightarrow np$ excitations of Li, Na, and K by positrons in the calculations of Hewitt et al. [21].

On the whole, the total cross section obtained from $\Sigma_E^{\rm pol} + \Sigma_E^{\rm Ps}$ has very little in common with that from just the polarization potential (Fig. 6, Table 2). The former has much greater magnitude, except in the low-energy limit, where the small scattering length $a \simeq 4.2$ from $\Sigma_E^{\rm pol} + \Sigma_E^{\rm Ps}$ produces $\sigma = 4\pi a^2 \simeq 220$ au. The inclusion of Ps formation produces a broad cross section maximum that is dominated by the *s*, *p*, *d*, and *f* partial waves, and has a sharper peak due to the *d*-wave resonance. Despite the very different centrifugal potential acting in these partial waves, the corresponding cross sections look relatively similar. This may be explained by the fact that the Ps-formation potential is probably strongest at $r \sim r_{\rm at} + r_{\rm Ps} \sim 5$, where $r_{\rm at} \sim 3$ [23] and $r_{\rm Ps} \sim 2$ are the

Table 2. Total and inelastic cross sections for positron scattering from Mg atoms.

k (au)	Energy (eV)	σ_{tot},[a] (10^{-16} cm^2)	σ_{tot},[b] (10^{-16} cm^2)	σ_{in},[b] (10^{-16} cm^2)
0.05	0.034	1335.0	96.5	0.0[c]
0.08	0.087	471.0	127.1	0.0
0.11	0.165	230.1	153.7	0.0
0.14	0.267	141.2	169.6	0.0
0.17	0.393	100.4	176.3	0.0
0.20	0.544	78.0	184.2	0.0
0.23	0.719	63.8	216.6	0.0
0.26	0.919	53.0	304.6	2.1
0.29	1.144	44.7	304.4	25.6
0.32	1.393	38.6	249.0	32.0
0.35	1.666	34.3	221.4	35.9
0.38	1.964	30.6	208.8	40.8
0.41	2.286	27.7	196.7	44.9
0.44	2.633	25.7	183.0	46.3
0.47	3.004	24.3	167.3	45.9
0.50	3.400	23.0	151.3	44.8
0.53	3.820	21.7	134.6	43.2
0.56	4.265	21.6	116.7	42.2
0.59	4.734	23.0	102.4	41.0
0.62	5.229	24.6	91.4	39.2
0.65	5.746	26.0	82.0	37.3
0.68	6.289	26.6	73.5	35.3
0.71	6.856	26.6	66.2	33.1
0.74	7.447	26.6	59.0	30.9
0.77	8.063	26.0	54.3	28.8
0.80	8.704	25.7	48.9	26.8
0.83	9.369	25.3	44.9	25.0
0.86	10.059	24.7	40.9	23.3
0.89	10.773	23.3	37.2	21.6

[a]Only the polarization potential Σ_E^{pol} taken into account.
[b]With the Ps-formation potential Σ_E^{Ps} added to Σ_E^{pol}.
[c]The Ps-formation threshold is at 0.843 eV, and the next ($3s \rightarrow 3p\ ^1P$ atomic excitation) threshold is at 4.19 eV (this Hartree–Fock value is close to the experimental 4.35 eV).

radii of Mg and Ps, respectively. Thus, the centrifugal barrier does not prevent the positron–atom interaction via the Ps-formation potential at $k \sim l/r \sim 0.2$, 0.4, 0.6 for $l = 1$, 2, 3. Indeed, these k values roughly correspond to those at which the corresponding partial cross sections peak (Fig. 6*b*). Of course, the polarization potential still dominates the long-range asymptotic behaviour and determines the low-energy expansion of the phase shifts (18). However, its magnitude at $r \sim 5$ ($\alpha/2r^4 \sim 0.07$ au is probably just comparable to that of Σ_E^{Ps}. It is clear from Fig. 6*b* that the sum over the partial waves for $k \gtrsim 0.7$ is by no means saturated by the first five l. The contributions of $l > 4$ are important to get the correct magnitude of the cross section, although they will not change the character of the cross section.

Also given in Table 2 is the reaction cross section σ_{in}. Below $E = 4.19$ eV it is the Ps-formation cross section. It peaks around $E = 3$ eV, and at $E = 3.82$ eV is built of 3, 21, 49, and 27% of the p, d, f, and g partial wave contributions (the s wave gives only about 0.04% of the total). The reaction cross section does not show any distinct features around the atomic excitation threshold, and towards larger energies (above 14 eV) becomes smaller than the excitation + ionization cross section obtained from Σ_E^{pol}. This again demonstrates the suppression of atomic excitations produced by the open Ps-formation channel.

4. Summary and conclusions

Low-energy positron scattering from Mg atoms has been calculated using many-body theory methods. This approach allowed us to calculate the effective interaction due to the polarization of the atom and due to the Ps formation separately, and to study the effect of Ps formation on the positron–atom interaction. We believe that for magnesium Ps formation is by far the largest, completely changing the character of the low-energy scattering cross sections. Qualitative agreement with the experimental data [8][2] seem to support this conclusion. This may be viewed as an indirect indication of the reality of positron–atom bound states obtained in the many-body calculations of Dzuba et al. [2].

The present calculation technique can be routinely extended to study the effect of Ps formation on positron scat-

tering from noble-gas atoms, where accurate experimental data for both the total and the Ps-formation cross sections exists. We also believe that Ps formation must have a large effect on positron scattering from other atoms of the second column of the periodic system (Zn, Cd, Hg), which are supposed to form bound states with positrons.

Acknowledgments

The authors would like to thank M. Yu. Kuchiev for useful discussions and W.E. Kauppila for communication prior to publication of their experimental results for positron scattering on Mg.

References

1. G.F. Gribakin and W.A. King. J. Phys. B: At. Mol. Opt. Phys. **27**, 2639 (1994).
2. V.A. Dzuba, V.V. Flambaum, V.A. Dzuba, G.F. Gribakin, and W.A. King. Phys. Rev. A, **52**, 4561 (1995).
3. I. Aronson, C.J. Kleinman, and L. Spruch. Phys. Rev. A: Gen. Phys. **4**, 841 (1971).
4. F.H. Gertler, H.B. Snodgrass, and L. Spruch. Phys. Rev. **172**, 110 (1968).
5. S. Golden and I.R. Epstein. Phys. Rev. A: Gen. Phys. **10**, 761 (1974).
6. M.W. Karl, H. Nakanishi, and D.M. Schrader. Phys. Rev. A: Gen. Phys. **30**, 1624 (1984).
7. S.P. Parikh, W.E. Kauppila, C.K. Kwan, R.A. Lukaszew, D. Przybyla, T.S. Stein, and S. Zhou. Phys. Rev. A, **44**, 1620 (1991).
8. J. Jiang, A. Surdutovich, W.E. Kauppila, C.K. Kwan, T.S. Stein, and S. Zhou. Can. J. Phys. (1996). This issue.
9. A.B. Migdal. Theory of finite Fermi-systems, and applications to atomic nuclei. Interscience Pub. New York. 1967.
10. L.V. Chernysheva, G.F. Gribakin, V.K. Inanov, and M. Yu. Kuchiev. J. Phys. B: At. Mol. Opt. Phys. **21**, L419 (1988).
11. M. Ya. Amusia, N.A. Cherepkov, L.V. Chernysheva, D.M. Davidovic, and V. Radojevic. Phys. Rev. A: Gen. Phys. **25**, 219 (1982).
12. M. Ya. Amusia and N.A. Cherepkov. Case Stud. At. Phys. **5**, 47 (1975).
13. H.P. Kelly. Phys. Rev. **171**, 54 (1968).
14. V.A. Dzuba and G.F. Gribakin. Phys. Rev. A: At. Mol. Opt. Phys. **49**, 2483 (1994); **50**, 3551 (1994).
15. V.A. Dzuba, V.V. Flambaum, and O.P. Sushkov. Phys. Lett. **140** A, 493 (1989).
16. G.F. Gribakin, B.V. Gul'tsev, V.K. Ivanov, and M. Yu. Kuchiev. J. Phys. B: At. Mol. Opt. Phys. **23**, 4505 (1990).
17. P.D. Burrow, J.A. Michejda, and J.-J. Comer. J. Phys. B: At. Mol. Opt. Phys. **9**, 3225 (1976).
18. N.I. Roman'uk et al. Pis'ma Zh. Tekh. Fiz. **6**, 877 (1980).
19. V.A. Dzuba, V.V. Flambaum, W.A. King, B.N. Miller, and O.P. Sushkov. Phys. Scripta T, **46**, 248 (1993).
20. R.N. Hewitt, C.J. Noble, and B.H. Bransden. J. Phys. B: At. Mol. Opt. Phys. **25**, 2683 (1992); **26**, 3661 (1993).
21. W.E. Kauppila, C.K. Kwan, T.S. Stein, and S. Zhou. J. Phys. B: At. Mol. Opt. Phys. **27**, L551 (1994).
22. M. Ya. Amusia and L.V. Chernysheva. Automated system for atomic structure calculations. Nauka, Leningrad. 1983.
23. A.A. Radtsig and B.M. Smirnov. Parameters of atoms and atomic ions: Handbook. Energoatomizdat, Moscow. 1986.
24. R. Szmytkowski and A.M. Alhasan. Phys. Scripta, **52**, 309 (1995).
25. T.F. O'Malley, L. Spruch, and L. Rosenberg. J. Math. Phys. **2**, 491 (1961).
26. R. Szmytkowski. J. Phys. II, **3**, 183 (1993).